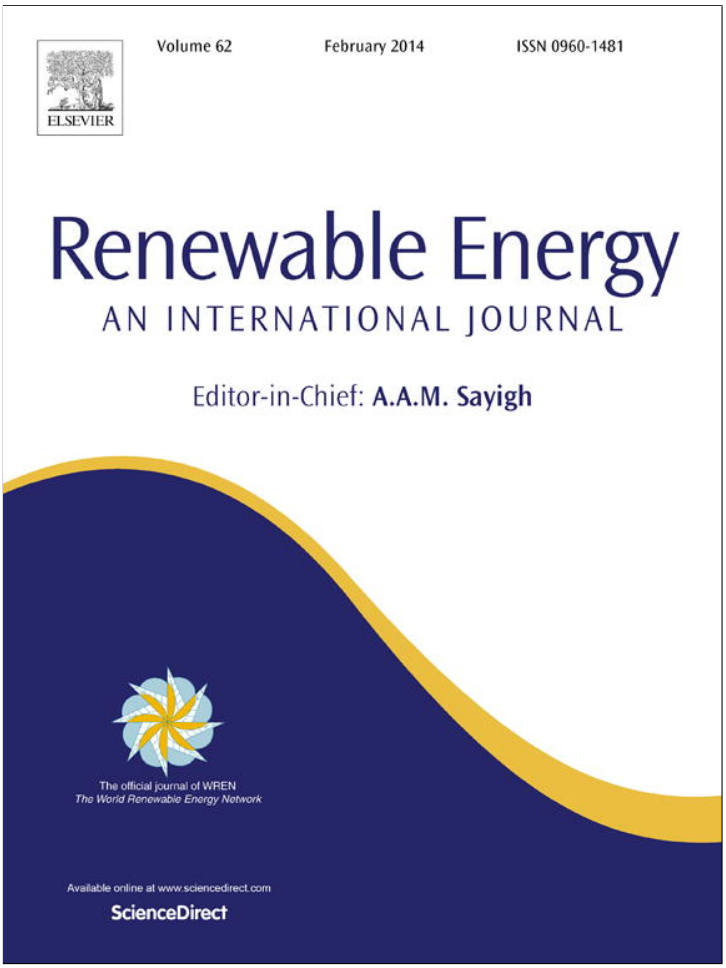

Renewable Energy 62 (2014) 619–628

Contents lists available at ScienceDirect

Renewable Energy

journal homepage: www.elsevier.com/locate/renene

Magnus type wind turbines: Prospectus and challenges in design and modelling

Ahmad Sedaghat*

Department of Mechanical Engineering, Isfahan University of Technology, Isfahan 84156-83111, Islamic Republic of Iran

ARTICLE INFO

Article history:
Received 8 February 2013
Accepted 19 August 2013
Available online 17 September 2013

Keywords:
Wind power
Magnus effect
Horizontal axis wind turbine
Potential flow
Blade element momentum theory

ABSTRACT

One of attracting concepts has been the use of Magnus effect to produce lift from rotating cylinders in various engineering applications. With emerging innovative Magnus type wind turbine technology, it is important to determine power performance and characteristics of such generators as correctly as possible. As stressed by Seifert, there is lack of theories in design and modelling of using Magnus force in engineering which is particularly noticed for the horizontal axis Magnus type wind turbines. In this study, the importance of research carried out for determining lift and drag forces of rotating circular cylinders is highlighted and reviewed. Then, the theoretical methods used in designing commercial aerofoil type wind turbines are extended to apply on the Magnus types. New formulation is presented for potential flow around the Magnus blades. The blade element momentum (BEM) theory is formulated for the Magnus wind turbines. A cubic function for angular induction factor is found from the BEM analysis which is strongly dependant on the drag to lift ratio. It is also observed that the relative wind incidence angle and the local power coefficient of the Magnus cylinder are independent functions of spin ratio.

1. Background introduction and literature review

The first successful device based on Magnus effect returns to the year1924, when Anton Flettner has manufactured the first ship operating with Magnus force using two large cylinders to propel his ship, Buckau. Since that success, the potential of producing high lift forces by rotating bodies in comparison with low lift force values of aerofoil type devices have attracted many researchers in different fields of Engineering. Many patents on Magnus effect were published in the areas of naval or aerospace applications [1]. Also, many researches have been focused on the production of aerodynamic forces from the rotating cylinders. But, very few Magnus devices were operated successfully [1].

Recently, the Flettner type rotor is becoming again a hot topic in naval engineering because of the energy costs and the rise of problems with climate change [1]. In the comprehensive review of the Magnus effect by Seifert [1], he believes "today, there are no specific methods available on how to design the lifting device of a rotor aeroplane or the rotor aeroplane airframe." This is particularly true on works reported especially on Magnus type wind turbines.

Bychkov et al. [2] has presented an experimental methodology on optimising a wind turbine equipped with rotating cylinders instead of traditional blades. He concluded that the optimal Magnus type wind turbine should possess 6 rotating cylinders (see Fig. 1) with high rotational speeds of 8000 rpm and the cylinders with high aspect ratio of 15. He believes his Magnus wind turbines can compete with the conventional wind turbines at low air speeds below 8 m/s. His findings suggest that the Magnus wind turbine can operate at as low as 1–2 m/s cut-in wind speeds which is crucially important for sites with low wind potentials.

More recently, Murakami and his co-workers [3,4] have patented a Magnus type wind turbine with 6 and 5 rotating cylinders which implemented some spiral ribs around the cylindrical blades. The wind turbine has been manufactured by Mecaro Co. in Japan [5].

In the Murakami [4] new patent in 2010, he indicated that their new Magnus wind turbine now operates with 5 spinning cylinders (see Fig. 2) and produces electrical power at cut-in wind speeds of above 4 m/s and at the rated wind speeds of 8 m/s which produces the net rated power of 3 kW. No data were given for higher wind speeds; although, the rotational speed is given to be 1080 rpm in their US patent [4].

Giudice and La Rosa [6] has designed and prototyped a chiral blade system (Magnus type) for hydroelectric microgeneration. Their experimental testing of low velocity flow is combined with some simple analytical approach based on the ideal potential flow solution for two-dimensional rotating cylinders. Their theoretical–experimental analysis suggested the great potential of the chiral

* Tel.: +98 311 391 2667, +98 913 167 6507 (mobile); Fax: +98 311 391 2628.
E-mail address: sedaghat@cc.iut.ac.ir.
URL: http://sedaghat.iut.ac.ir/

0960-1481/$ – see front matter © 2013 Elsevier Ltd. All rights reserved.
http://dx.doi.org/10.1016/j.renene.2013.08.029

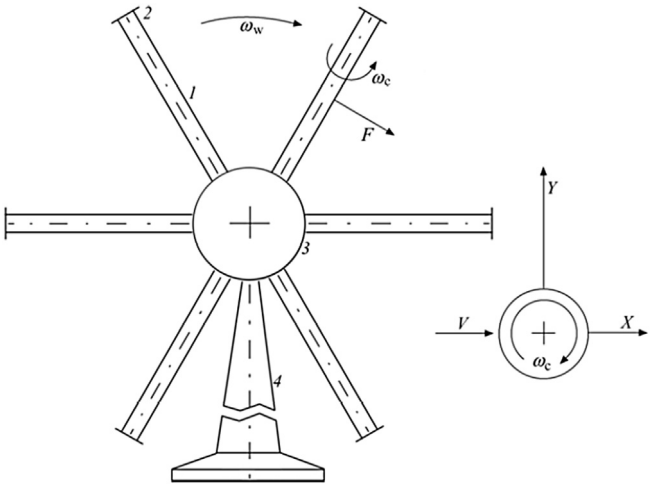

Fig. 1. The suggested optimum horizontal axis Magnus wind turbine with 6 rotating circular cylinders with high rotational speeds of 8000 rpm [2].

device with regard to both wind and hydro power generation particularly for the low head water flow conditions such as rivers without dams, tidal streams and ocean currents.

Perhaps one of the first experiments on rotating cylinders dated back as early as 1925 by Reid [7] for application in aeroplane design. The report by Reid [7] summarised the results of flow over smooth cylinders at various wind speeds and rotational speeds up to 3600 rpm concluding considerable increase in lift force. The boundary layer theory over rotating circular cylinders was studied in 1957 by Glauert [8]. In 1983, Ingham [9] reported his computational results for very small Reynolds number flows around the rotating cylinders. In his works, the viscous flow was studied over rotating cylinders. Mittal and Bhaskar [10] have reported two-

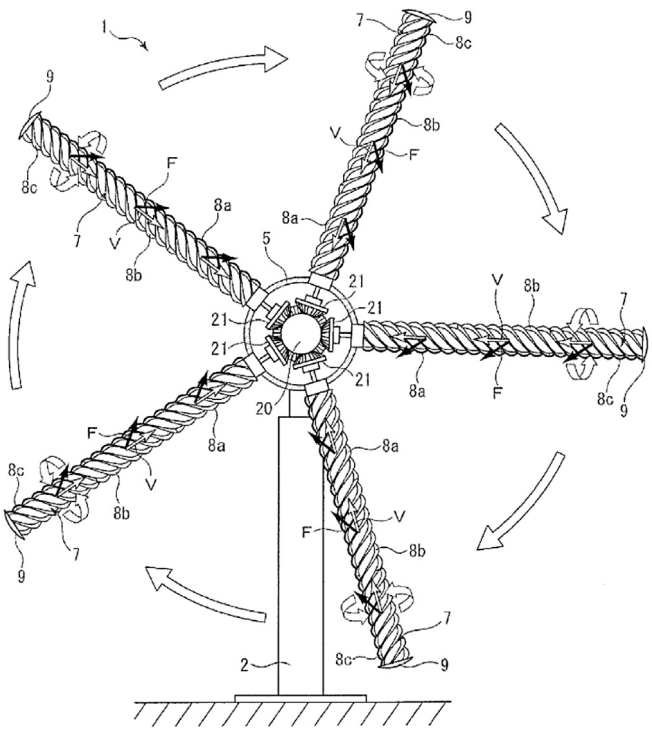

Fig. 2. The new horizontal axis Magnus wind turbine manufactured with 5 rotating circular cylinders with helical ribs by Murakami et al. [4].

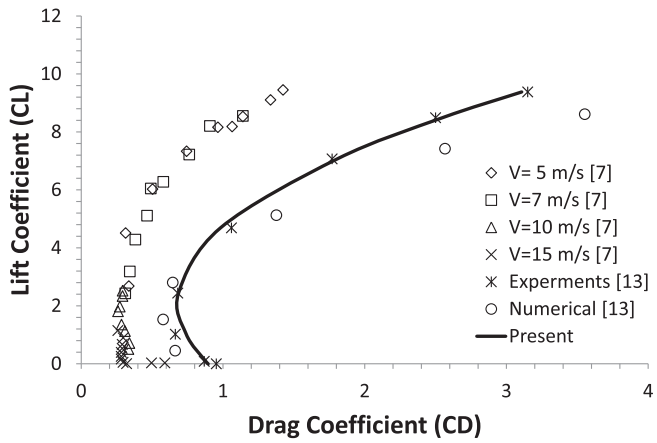

Fig. 3. Variation of lift coefficient versus drag coefficient at different wind speeds for the rotating circular cylinder.

dimensional Navier–Stokes simulations for flow over a spinning circular cylinder with the Reynolds number of 200. The dimensionless spin ratio $\acute{\omega}$ was varied between 0 and 5. Vortex shedding was observed for $\acute{\omega} < 1.91$. For higher spinning rates, they observe that flow achieves a steady state condition except for $4.34 < \acute{\omega} < 4.70$ where the flow becomes unstable again. For high rotation rates, they have reported that very large lift coefficients can be obtained via the Magnus effect; however, they concluded that the power requirement for rotating the cylinder increases rapidly with the spinning rate.

In real steady-state flows, vorticity created at the solid wall is convected and diffused. Prandtl believed that the equilibrium state at $\acute{\omega} = 2$, dictate the lift values at higher rotational rates to the maximum value of $C_{Lmax} = 4\pi \approx 12.6$. However, experimental and numerical observations by Tokumaru and Dimotakis [11] suggest that the maximum lift limit can be far higher at higher aspect ratios and higher rotational speeds due to unsteady effects. Experimental and numerical works for large Reynolds numbers $4 \times 10^4 < \mathrm{Re} < 6.6 \times 10^5$ by Refs. [12,13] suggest that $2 < \acute{\omega} < 4$ may be a proper range for using Magnus effects in wind turbines whilst avoiding higher values of drag coefficient at higher rotational speeds. However, the monotonic increase of lift coefficient over the rotating cylinders may not be maintained due to instabilities, 3D effects, and centrifugal forces. Some computational evidences based on simulating Navier–Stokes equations show the instability and violation of maximum lift at high Reynolds numbers and high spin rates, simultaneously.

The purpose of this study is however to mimic the numerous experimental and computational findings on lift and drag forces over rotating circular cylinders into the theories developed for the horizontal axis wind turbines and to examine possibility of using Magnus effect in wind turbine applications. These theories include potential flow analysis, the one-dimensional linear and angular momentum concepts, and the blade element theory incorporated with the blade element momentum (BEM) which are discussed and extended for application in design and modelling of the horizontal axis Magnus type wind turbines.

2. Experimental measurements on lift and drag of spinning cylinders

Fluid dynamics of flows around spinning cylinders is fairly complicated and features many interesting phenomena depending on flow regime characterised by the Reynolds number $\mathrm{Re} = V \infty D/\nu$ and the spinning ratio $\acute{\omega} = \omega D/2V\infty$. According to numerous

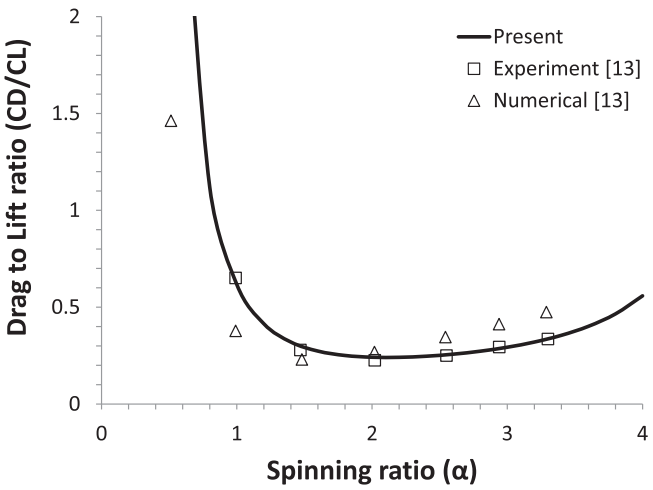

Fig. 4. Drag to lift ratio against spinning ratio for the rotating circular cylinder.

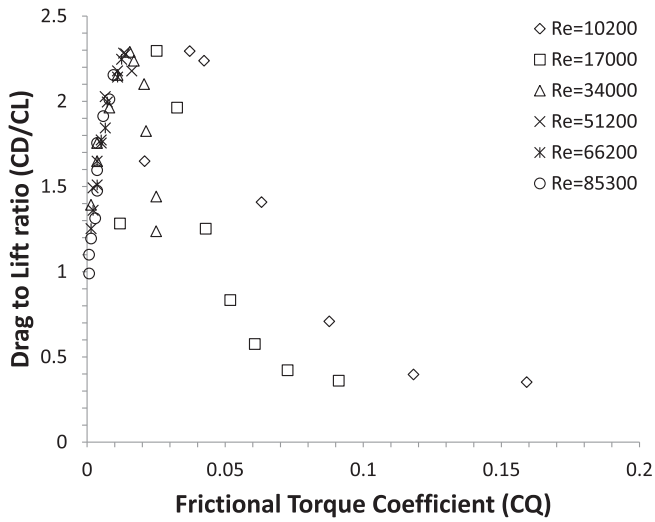

Fig. 5. Drag to lift ratio variation against frictional torque coefficient for the spinning circular cylinder [14].

experimental and numerical studies, the magnitude of the lift and drag forces and also friction torque depends on the spinning ratio ώ and the Reynolds number [1,7,13]. Fig. 3 summarises variation of Lift coefficient (C_L) of a rotating circular cylinder versus Drag coefficient (C_D) at relatively high Reynolds number ($10^4 \le \mathrm{Re} \le 10^5$) and the spinning ratio of $0 \le \acute{\omega} \le 4$ [13] which is also correlated with the following polynomial fit.

$$C_L = -0.01355 - 0.4065\acute{\omega} + 1.2944\acute{\omega}^2 + 0.2249\acute{\omega}^3 - 0.09632\acute{\omega}^4$$
$$C_D = 1.0631 - 0.9137\acute{\omega} + 0.4694\acute{\omega}^2 \tag{1}$$

The relation between lift and drag forces may also expressed as

$$C_D = 0.8954 - 0.1988C_L + 0.04634C_L^2 \tag{2}$$

Although the above relations will not provide general relations for the lift and the drag distribution for the spinning circular cylinders, it provides useful relations for the purpose of current study. The results of the experimental and numerical works of [13] and [7] together with the above correlated fits (1) and (2) are shown in Fig. 4.

Fig. 4 shows the comparison of lift to drag ratio (C_D/C_L) against the spinning ratio reported in Ref. [13] also correlated with relations (1). The lift to drag ratio possess minimum value within the range of $1.5 \le \acute{\omega} \le 2.5$; this range may be considered as the optimum range for utilising the spinning cylinder in Magnus type wind turbine.

For efficient Magnus type wind turbine operation, the power input to the rotating cylinders must be reduced to minimum. Recent experimental study [14] on friction coefficient of rotating circular cylinders has revealed that the corresponding torque coefficient (C_Q) may attain its minimum within the spinning range of $0.5 \le \acute{\omega} \le 1.5$ and $1.7 \times 10^4 \le \mathrm{Re}$. But, at these range of the Reynolds number and spinning ratio, the drag to lift ratios are considerably high, i.e. $1.0 \le C_D/C_L \le 2.5$, as shown in Fig. 5.

More experimental or numerical results are needed to find an optimum range for the spinning ratio and the Reynolds number; however as a compromise, we may suggest the range of spinning ratio to $1.5 \le \acute{\omega} \le 2.5$ and the Reynolds number within $1.7 \times 10^4 \le \mathrm{Re} \le 3.4 \times 10^4$ for designing an efficient Magnus type wind turbine. In fact, this may be improved later when more experimental or numerical results become available.

3. The methodologies and mathematical development

3.1. Potential flow around rotating circular cylinders

For irrotational, incompressible and inviscid flows the Laplace equation is valid for the velocity potential, φ. The solution to the Laplace equation is referred as the potential flow solution. The velocity potential can be obtained for flows around aerodynamic bodies by combining the simple ideal flows known as uniform flow, source and sink, doublet, and vortex flows. For the potential flow around a rotating circular cylinder, the combination of velocity potentials for a uniform flow, a doublet at the centre of the cylinder, and a vortex is used as expressed here. The results of the potential theory for the velocity potential for the flow around the spinning cylinder is given by Ref. [15]

$$\varphi = U_\infty r\left(1 + \frac{r_c^2}{r^2}\right)\cos\theta - \frac{\Gamma}{2\pi}\theta \tag{3}$$

where U_∞ is the uniform freestream velocity, r_c is the radius of the circular cylinder,Γ is the circulation for clockwise spin of the cylinder, and (r, θ) are the cylindrical coordinate system measured from the centre of cylinder. The velocity components around the cylinder in the cylindrical coordinate system is then obtained by

$$u_r = \frac{\partial\varphi}{\partial r} = U_\infty\left(1 - \frac{r_c^2}{r^2}\right)\cos\theta \tag{4}$$

$$u_\theta = \frac{1}{r}\frac{\partial\varphi}{\partial\theta} = -U_\infty\left(1 + \frac{r_c^2}{r^2}\right)\sin\theta - \frac{\Gamma}{2\pi r} \tag{5}$$

On the surface of the cylinder ($r = r_c$), it is seen from the equations (4) and (5) that the radial velocity is $u_r = 0$ and the tangential velocity is determined by

$$u_\theta = -2U_\infty\sin\theta - \frac{\Gamma}{2\pi r_c} \tag{6}$$

The surface pressure, p, is obtained from the Bernoulli equation, by inserting the tangential velocity on the surface of the cylinder from equation (6), as follows

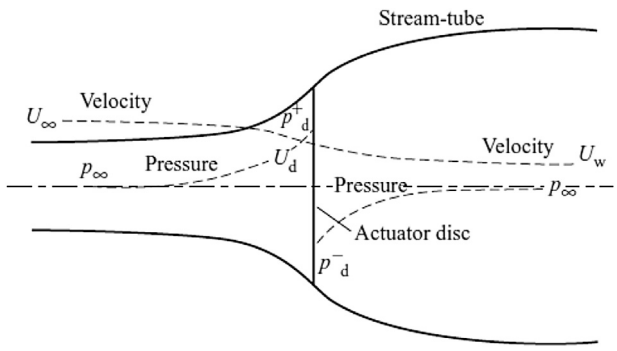

Fig. 6. Actuator disk model of a wind turbine in a stream tube [16].

$$p_\infty + \frac{1}{2}\rho U_\infty^2 = p + \frac{1}{2}\rho\left(-2U_\infty \sin\theta - \frac{\Gamma}{2\pi r_c}\right)^2 \tag{7}$$

or

$$p = p_\infty + \frac{1}{2}\rho U_\infty^2\left(1 - 4\sin^2\theta - \frac{2\Gamma\sin\theta}{\pi r_c U_\infty} - \frac{\Gamma^2}{4\pi^2 r_c^2 U_\infty^2}\right) \tag{8}$$

Integrating the surface pressure to obtain the drag and lift forces applied on the spinning circular cylinder, one may obtain

$$F_L = F_y = -\int_0^{2\pi} \Delta p \sin\theta r_c d\theta = \rho U_\infty \Gamma \tag{9}$$

$$F_D = F_x = -\int_0^{2\pi} \Delta p \cos\theta r_c d\theta = 0 \tag{10}$$

which clearly shows that the drag force cannot be obtained from the analysis of the potential flow due to assumption of inviscid fluid flow. For an incompressible fluid flow with constant density, the lift force is a function of the freestearm velocity U_∞ and the circulation Γ around the cylinder. The lift and drag coefficients are subsequently obtained using following relations:

$$C_L = \frac{F_L}{\frac{1}{2}\rho U_\infty^2 A} \tag{11}$$

$$C_D = \frac{F_D}{\frac{1}{2}\rho U_\infty^2 A} \tag{12}$$

where A is a reference area, usually taken as the projected area perpendicular to the flow direction for blunt bodies; here for the cylinder with unit length, the reference area is taken equals to $A = 2r_c \times 1$.

3.2. The actuator disk model

Considering the rotor of a horizontal axis wind turbine with infinite number of rotating circular cylinders with near zero thickness of the rotor blades, an actuator disk model is the mathematical representation of such wind turbine rotor. In the actuator disk model, it is assumed that a sudden drop occurs in pressure just across the rotor area whilst air speed remains constant at the rotor area [16]. Fig. 6 shows the actuator disk model of a wind turbine in a stream tube.

From the conservation law of the mass flow rate within the stream tube, it is realised that the mass flow rate must be the same everywhere along the stream tube given by

$$\dot{m} = \rho A_\infty U_\infty = \rho A_d U_d = \rho A_w U_w \tag{13}$$

The symbol ∞ refers to freestream condition, d refers to flow condition at the actuator disc and w refers to far wake flow condition.

It is generally assumed that the actuator disc induces velocity components in both axial and tangential directions which must be taken into account when determining the relative wind speed over the blade sections. The axial component of this induced flow at the disc is given by $-aU_\infty$, where a is called the axial flow induction factor. Therefore at the disc, the net axial velocity is determined by

$$U_d = U_\infty(1-a) \tag{14}$$

For the spinning cylinders, in clockwise direction, the flow particles passing over the cylinder are accelerated while the flow particles under the cylinder are decelerated. Thus, the induced velocity in tangential direction due to rotation of the blade should take into account both wake rotation and also the spin of blade sections. This is discussed in details in Section 3.2.2.

3.2.1. Conservation law on linear momentum

From the conservation law of linear momentum for the one-dimensional stream tube shown in Fig. 6, the rate of change of momentum of the air that passes through the actuator disc equals to the net forces causing this change. The overall change of velocity, $U_\infty - U_w$, times the mass flow rate gives the rate of change of momentum, i.e. $(U_\infty - U_w)\rho A_d U_d$. The net force comes entirely from the pressure drop across the actuator disc; therefore, the conservation law of the linear momentum is given using equation (14) as

$$\left(p_d^+ - p_d^-\right)A_d = U_\infty(1-a)\rho A_d U_\infty(1-a) \tag{15}$$

To obtain the pressure drop, $(p_d^+ - p_d^-)$, Bernoulli's equation is applied separately to the upstream and downstream sections of the stream-tube which yields to [16]

$$\left(p_d^+ - p_d^-\right)A_d = \frac{1}{2}\rho\left(U_\infty^2 - U_w^2\right) \tag{16}$$

Equating the right hand sides of equations (15) and (16), one may obtain

$$U_w = U_\infty(1-2a) \tag{17}$$

Hence, the net force of wind on the actuator disk model is calculated as

$$F = \left(p_d^+ - p_d^-\right)A_d = 2\rho A_d U_\infty^2 a(1-a) \tag{18}$$

Since the rate of work done by the force on the actuator disk, FU_d, is equals to the power extracted from the wind, the net power of the wind turbine is determined by

$$P = FU_d = 2\rho A_d U_\infty^3 a(1-a)^2 \tag{19}$$

and the corresponding power coefficient which is an important characteristic of any wind turbine is determined as

$$C_P = \frac{P}{\frac{1}{2}\rho U_\infty^3 A_d} = 4a(1-a)^2 \tag{20}$$

From the Betz theory, an ideal wind turbine reduces wind speed to two third of the freestream value. Thus, the maximum value of

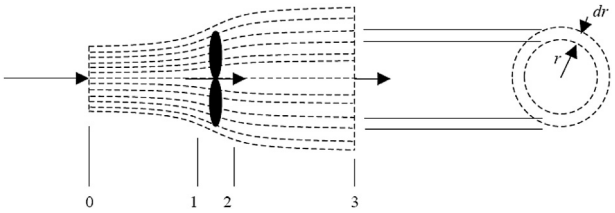

Fig. 7. Annular control volumes for calculating wake rotation.

the power coefficient can be calculated from equation (20) by substituting the optimum value of $a = 1/3$ which yields to the maximum power capture of $C_{P\max} = 16/27 = 0.593$ from the wind turbine which is also known as the Betz limit [16].

3.2.2. Conservation law on moment of momentum

A wind turbine produces a useful torque for generating power; the conservation of moment of momentum must be satisfied by employing a wake rotation downstream of the wind turbine in some annular control volumes as shown in Fig. 7.

Associated with the loss of axial momentum is a loss of angular momentum. Exertion of a torque on the rotor disc by the air requires an equal and opposite torque to satisfy the conservation of moment of momentum in the stream tube. The consequence of the reaction torque is the rotation of air in opposite direction of the rotor; hence, the air gains angular momentum and the air particles attain axial and tangential components of velocity. The additional tangential velocity is imposed due to the spin of the cylinder along its axis and the overall velocity components of the air particles passing over the cylinder is then given as shown in Fig. 8. The change in tangential velocity is expressed in terms of the angular induction factor $\acute{a}$.

Each Magnus cylindrical blade with circular cross section of the radius r_c rotates with the spin of ω about its axis. As shown in Fig. 8, by assuming a uniform axial inflow, in vicinity downstream of the actuator disc, the tangential velocity contains two parts. One part is $2\Omega r\acute{a}$ due to the blade angular movement in the plane of rotor with Ω as the rotor angular velocity and r as the radial distance from the rotor axis of rotation. Second part, ωr_c, as differs between Magnus and conventional aerofoil type wind turbines, represents the wake reaction to the induced tangential velocity of each cylinder due to spinning about its axis (see Fig. 8). Hence, the air axial velocity is $U_\infty(1-a)$ and the tangential velocity is $2\acute{a}\Omega r - \omega r_c$ just slightly downstream of the actuator disk. It is also generally assumed that at the middle of the actuator disc thickness, over the blade itself, the tangential velocity equals to the half value expressed just downstream of the wind turbine, i.e.$\Omega r\acute{a} - \omega r_c/2$, in direction of rotor motion.

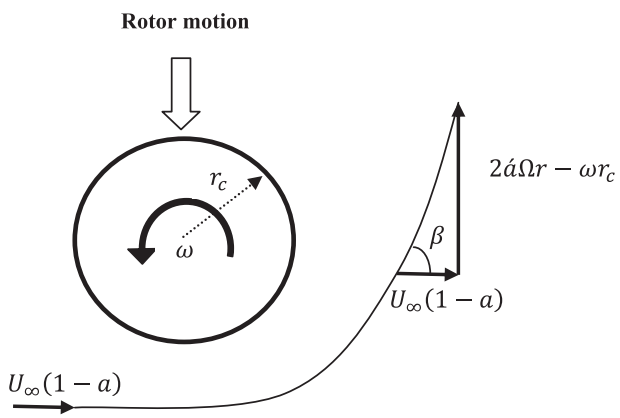

Fig. 8. The velocity components just downstream of the actuator disk model.

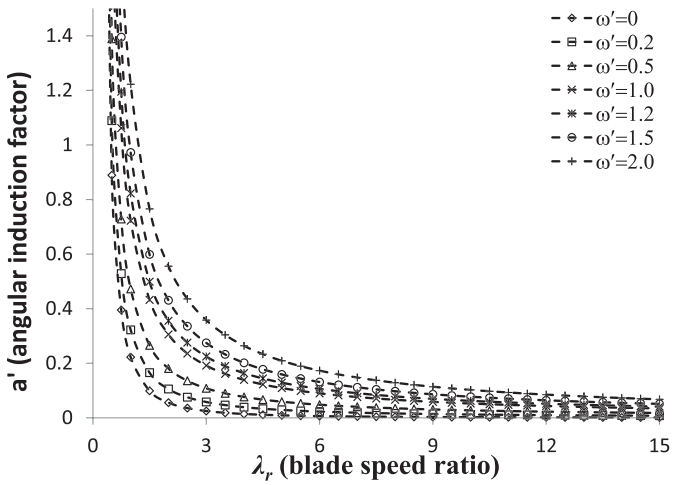

Fig. 9. The variation of the angular induction factor against the blade speed ratio at different values of the spin ratio.

The torque exerted on the annular control volume at the radius r with radial thickness of dr as shown in Fig. 7 will be equal to the rate of change of angular momentum of the air passing through it. Thus, the torque is obtained by the product of the mass flow rate $(\rho\delta A_d U_\infty(1-a))$, times the change of tangential velocity $(2\Omega\acute{a}\, r - \omega r_c)$, times the radius of the annular control volume (r); as follow:

$$\delta Q = \rho\delta A_d U_\infty(1-a) \times \left(2\Omega\acute{a}r - \omega r_c\right) \times r \tag{21}$$

where δA_d is the area of the annular ring, the driving torque on the rotor shaft is δQ, and the corresponding output shaft power is determined by

$$\delta P = \Omega\delta Q = \rho\delta A_d U_\infty(1-a)\left(2\Omega^2\acute{a}r^2 - \omega\Omega r_c r\right) \tag{22}$$

Rewriting equation (19) for the annular control volume shown in Fig. 7 and by equating the results with the value obtained from the moment of momentum analysis for the elemental power given in equation (22), it may follow that

$$2\rho\delta A_d U_\infty^3 a(1-a)^2 = \rho\delta A_d U_\infty(1-a)\left(2\Omega^2\acute{a}r^2 - \omega\Omega r_c r\right) \tag{23}$$

or

$$2U_\infty^2 a(1-a) = 2\Omega^2\acute{a}r^2 - \omega\Omega r_c r \tag{24}$$

Defining the dimensionless parameters including the blade speed ratio as, $\lambda_r = r\Omega/U_\infty$, and the cylinder spin ratio as, $\acute{\omega} = (r_c\omega/U_\infty)$, a relation may be obtained among the axial induction factor, the angular induction factor, and the spin ratio as follow

$$a(1-a) = \lambda_r^2\acute{a} - \frac{\acute{\omega}}{2}\lambda_r \tag{25}$$

The angular induction factor then can be determined by rearranging equation (25) to give

$$\acute{a} = \frac{1}{\lambda_r^2}\left[a(1-a) + \frac{\acute{\omega}}{2}\lambda_r\right] \tag{26}$$

The variation of the angular induction factor against the blade speed ratio at different values of the spin ratio, $\acute{\omega}$, and by using the

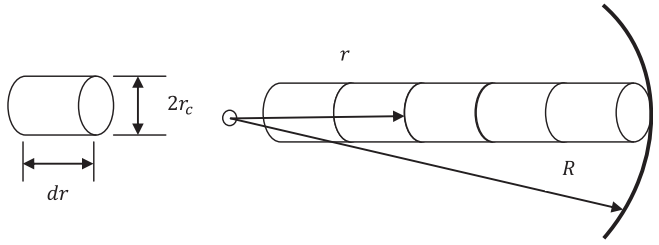

Fig. 10. The elemental constitution of a Magnus wind turbine blade.

optimum value of the axial induction factor, i.e. $a = 1/3$, is shown in Fig. 9 which shows a decreasing function of λ_r. The spin ratio, $\acute{\omega}$, has also increasing effect on the angular induction factor values.

The elemental power in equation (22) is then can be rewritten using equation (26) to give

$$\delta P = \left(\frac{1}{2}\rho U_\infty^3 2\pi r dr\right) 4(1-a)\left(\lambda_r^2 \acute{a} - \frac{\acute{\omega}}{2}\lambda_r\right) \tag{27}$$

which is expressed in dimensionless form as the power coefficient given by

$$\frac{dC_P}{dr} = \frac{\delta P/dr}{\frac{1}{2}\rho U_\infty^3 \pi R^2} = \frac{4\pi\rho U_\infty^3 (1-a) r\left(\lambda_r^2 \acute{a} - \frac{\acute{\omega}}{2}\lambda_r\right)}{\frac{1}{2}\rho U_\infty^3 \pi R^2} \tag{28}$$

Defining a dimensionless parameter for the radial length of rotor blades by $\mu = r/R$, with R as the tip radius of the blade from the centre of rotation, the differential form of the power coefficient with respect to μ is given by

$$\frac{dC_P}{d\mu} = 8(1-a)\left(\mu^3\lambda^2 a' - \frac{\omega'}{2}\mu^2\lambda\right) \tag{29}$$

For the optimum value of the induction factor, i.e. $a = 1/3$, it is shown that the maximum power extraction from the wind turbine is the same as for the non-rotating wake condition [17]. Hence, equation (26) is rewritten as $\acute{a} = (1/\lambda^2\mu^2)[(2/9) + (1/2)\acute{\omega}\lambda\mu]$ and is substituted into the relation (29) to be integrated along the rotor radius. It is interestingly seen that for all the values of $\acute{\omega}$ and λ the total power obtained from this wind turbine is equals to the maximum power in the limit of Betz, i.e.

$$C_P = \int_0^1 8(1-a)\left(\mu^3\lambda^2\acute{a} - \frac{\acute{\omega}}{2}\mu^2\lambda\right)d\mu = \int_0^1 \frac{32}{27}\mu d\mu = \frac{16}{27} \tag{30}$$

This further proofs correctness of the above analyses for the Magnus wind turbine with rotating circular cylinders which is consistence with the general theories developed for the commercial aerofoil type wind turbines on not violating the Betz limit. The obtained optimum values for a and $\acute{a}$ lead to the maximum power capture from the Magnus wind turbine.

3.3. The blade element model

In actuator disk theory, friction drag is ignored which is not realistic. In order to modify this shortcoming [17], blade element theory is considered to incorporate the effects of drag force exerted on each elemental constitution of blade as shown in Fig. 10. The design with wake rotation took into account the generation of rotational kinetic energy in the wake, which resulted in less energy extraction by the rotor than it would be expected without wake rotation.

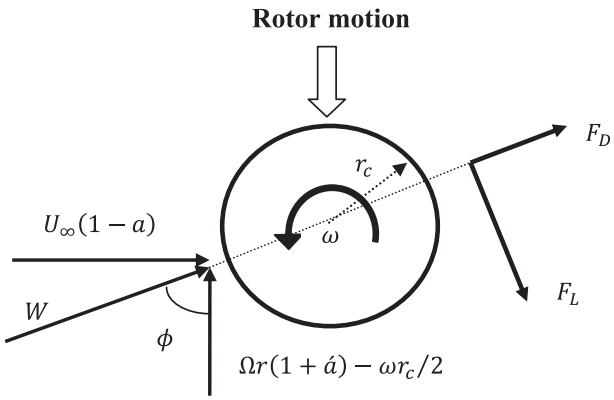

Fig. 11. The wind velocity components over the blade element of Magnus wind turbine.

Here, it is assumed that the forces acting on the cylinder blade elements can be calculated by means of two dimensional lift and drag forces measured for rotating circular cylinders and calculating the relative wind angle, φ, of the resultant velocity on the plane of the element as shown in Fig. 11. The velocity component in the radial direction due to centrifugal forces and three-dimensional effects are ignored here.

The velocity components on the plane of the element of the circular cylinder blade at a radial position should now be expressed by the freestream wind speed, the axial and angular induction factors, the rotational speed of the rotor, and the spin of the cylinder itself. The values of the lift and drag coefficients may be obtained based on the spin of the circular cylinder from available experimental results or some correlations to relate the drag force to the lift force obtained from the inviscid analysis discussed in the section 3.1.

Consider a horizontal axis wind turbine with B rotating circular cylinders with radius of r_c and the rotor blades with tip radius of R. In the conventional aerofoil type wind turbines design both the chord length and the pitch angle may vary along the blade span. However, for the Magnus type wind turbines, the chord length (or cylinder diameter$2r_c$) may be fixed along the blade. Consider now that the Magnus rotor operates with the angular velocity of Ω, the cylinder spin of ω, and the wind speed of U_∞. The net tangential flow velocity over the blade element includes the tangential velocity $r\Omega$, of the blade element, the tangential velocity of the wake $\acute{a}r\Omega$, and half the value of the spin of cylinder $\omega r_c/2$, i.e. $(1+\acute{a})r\Omega - \omega r_c/2$. The velocity components and forces acting on a cross section of the Magnus wind turbine are shown in Fig. 11.

Hence, the resultant relative velocity over the blade element is determined as

$$W = \sqrt{U_\infty^2(1-a)^2 + \left(\left(1+\acute{a}\right)r\Omega - \omega r_c/2\right)^2} \tag{31}$$

and the relative wind incidence angle with respect to the plane of rotor motion is obtained as

$$\phi = \tan^{-1}\left(\frac{U_\infty(1-a)}{\left(1+\acute{a}\right)r\Omega - \omega r_c/2}\right) = \tan^{-1}\left(\frac{1-a}{\left(1+\acute{a}\right)\lambda_r - \acute{\omega}/2}\right) \tag{32}$$

where $\lambda_r = r\Omega/U_\infty$ is the blade speed ratio. Inserting the angular induction factor from the equation (26) into the above relation (32), the relative wind incidence angle φ is determined as an independent function of the cylinder spin ratio which is simplifies as

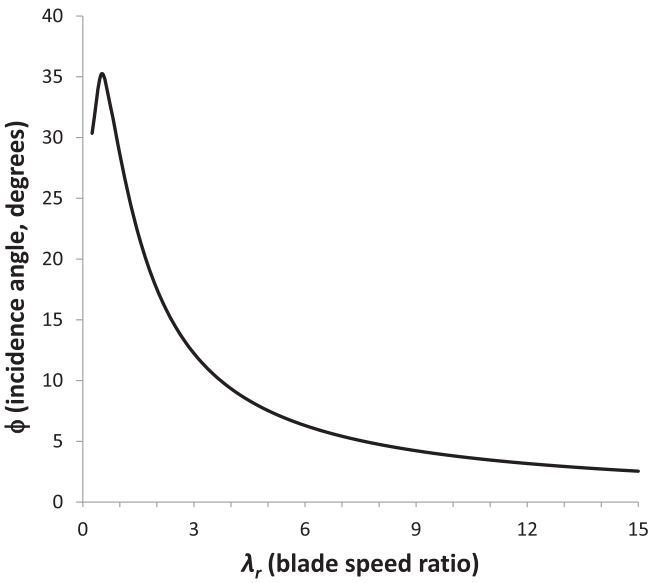

Fig. 12. The variation of the wind incidence angle against the blade speed ratio for the Magnus wind turbine using inviscid momentum theory.

$$\phi = \tan^{-1}\left(\frac{1-a}{\lambda_r + \frac{a(1-a)}{\lambda_r}}\right) \tag{33}$$

The optimum distribution of the incidence angle φ for the Magnus wind turbine is shown in Fig. 12 with using the optimal value of the axial induction factor, i.e. $a = 1/3$. Fig. 12 shows that the relative wind angle attains its maximum at the blade speed ratio of 0.5 with a value of 35°. This distribution of the relative wind incidence angle φ is however based on the inviscid flow assumption that is later modified to include the effects of viscosity and the corresponding drag force over the blade using BEM theory.

Moreover from the Fig. 11, the tangential force F_T which generates the rotor torque and the normal force F_N which contribute to the rotor thrust force are determined by

$$\begin{aligned} F_T &= F_L \sin\phi - F_D \cos\phi \\ F_N &= F_L \cos\phi + F_D \sin\phi \end{aligned} \tag{34}$$

The lift F_L and the drag F_D forces can be determined using the potential flow solution or more accurately using experimental values in the BEM theory which is discussed in section 3.4.

3.3.1. The potential flow solution for the lift and the drag forces

Employing the Bernouli equation, the pressure distribution over the spinning circular cylinders of the Magnus wind turbines can be determined by

$$\begin{aligned} \Delta p &= \tfrac{1}{2}\rho U_\infty^2 \left[1 - \frac{u_\theta^2}{U_\infty^2}\right] \\ u_\theta &= -2W\sin\left(\theta + \tfrac{\pi}{2} - \phi\right) + r_c\omega \end{aligned} \tag{35}$$

where u_θ is the tangential component of velocity on the surface of the spinning cylinder. The term u_θ^2/U_∞^2 can be expressed using (31) and (32) as follow

$$\begin{aligned} \frac{u_\theta^2}{U_\infty^2} &= \left(\dot{\omega} - 2X\sin\left(\theta + \tfrac{\pi}{2} - \phi\right)\right)^2 \\ X &= \frac{W}{U_\infty} = (1-a)\sqrt{1+\cot^2\phi} \end{aligned} \tag{36}$$

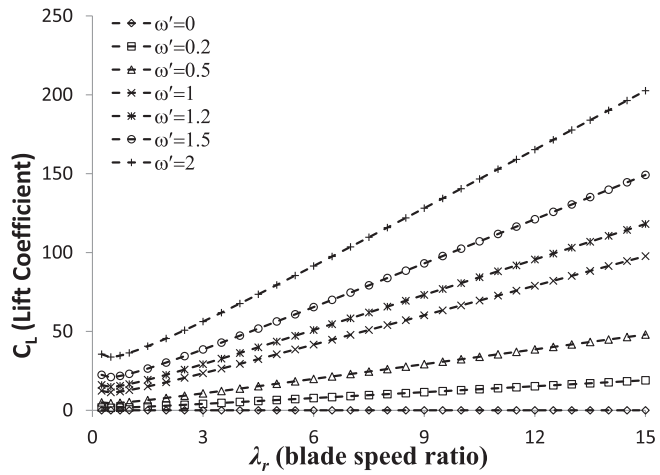

Fig. 13. The variation of lift coefficient against the blade speed ratio at different values of the dimensionless rotational speed of the cylinder from the inviscid momentum theory.

Hence, the lift and drag forces in equations (9) and (10) can be rewritten over the cylinder as

$$F_L = -\int_0^{2\pi} \Delta p \sin\left(\theta + \frac{\pi}{2} - \phi\right) r_c \mathrm{d}\theta \tag{37}$$

$$F_D = -\int_0^{2\pi} \Delta p \cos\left(\theta + \frac{\pi}{2} - \phi\right) r_c \mathrm{d}\theta \tag{38}$$

Using (35) and the lift and drag coefficients given in (11) and (12), one may obtain

$$\begin{aligned} C_L &= \frac{F_L}{\frac{1}{2}\rho U_\infty^2 A} = \frac{1}{2}\int_0^{2\pi}\left[1 - \left(\dot{\omega} - 2X\sin\left(\theta + \frac{\pi}{2} - \phi\right)\right)^2\right]\sin\left(\theta + \frac{\pi}{2} - \phi\right)\mathrm{d}\theta \\ &= \frac{\pi\dot{\omega}}{\lambda_r}\sqrt{4\lambda_r^4 + 4\dot{\omega}\lambda_r^3 + 4\left(1 - a^2 + \dot{\omega}^2\right)\lambda_r^2 + 4a\dot{\omega}(1-a)\lambda_r + 4a^2(a-1)^2} \end{aligned} \tag{39}$$

$$\begin{aligned} C_D &= \frac{F_D}{\frac{1}{2}\rho U_\infty^2 A} \\ &= -\frac{1}{2}\int_0^{2\pi}\left[1 - \left(\dot{\omega} - 2X\sin\left(\theta + \frac{\pi}{2} - \phi\right)\right)^2\right]\cos\left(\theta + \frac{\pi}{2} - \phi\right)\mathrm{d}\theta = 0 \end{aligned} \tag{40}$$

The lift coefficient calculated here is dependent on the blade speed ratio, λ_r, the axial induction factor, a, and the dimensionless spin ratio, $\dot{\omega}$. For the optimum induction factor, $a = 1/3$, the distribution of the lift coefficient against λ_r for different values of $\dot{\omega}$ is shown in Fig. 13. It is seen that the rotational speed $\dot{\omega}$ as well as the blade speed ratio, λ_r, have increasing effect on the lift coefficient. Comparing with the two-dimensional results of the lift force $\rho U_\infty \Gamma$ over a circular cylinder, which is a constant value for a given wind speed and spin of the cylinder, the relative wind speed $W = \sqrt{U_\infty^2(1-a)^2 + ((1+a')r\Omega - \omega r_c/2)^2}$ is an increasing variable along the rotor blade of the Magnus wind turbine, and therefore, the lift coefficient increases along the rotor blade from

root to tip. Therefore, the larger the aspect ratio of the blade the higher values of the lift force is expected. The spin of rotor can also considerably increase the lift force particularly towards the tip of the Magnus blade. Similarly as expected, the drag coefficient is calculated to be zero from this inviscid potential flow analysis.

3.4. The blade element momentum (BEM) theory

The BEM theory assumes a two dimensional structure of flow over the blade element which solely assumes the elemental lift and drag forces are responsible for the change of momentum of the air passing the annular swept area by the rotor element. Therefore, the radial interaction between the flow and the rotor is ignored that is only true if the axial flow induction factor remain constant in radial direction. In practice, there are conditions that confirm validity of this assumption (see [17]).

For the Magnus wind turbine with B number of rotating circular cylinders, the elemental axial force over B number of blade elements is given by

$$dF_N = dF_L\cos\phi + dF_D\sin\phi = \frac{1}{2}\rho W^2 B(2r_c)(C_L\cos\phi + C_D\sin\phi)dr \tag{41}$$

From the linear momentum theory discussed in section 3.2.1, the axial force exerted on the actuator disk is equals to the rate of change of axial momentum of the air passing through the swept annulus shown in Fig. 7 as follow

$$dF_N = \left(p_d^+ - p_d^-\right)dA_d = 4\pi\rho U_\infty^2 a(1-a)rdr \tag{42}$$

The wake rotation and the cylinder spin also contribute to the drop in the wake pressure by increasing in dynamic head, which is

$$\frac{1}{2}\rho\left(2\acute{a}\Omega r - \omega r_c\right)^2$$

Thus, the extra axial momentum of air on the annular area is

$$\frac{1}{2}\rho\left(2\acute{a}\Omega r - \omega r_c\right)^2 dA_d = \pi\rho\left(2\acute{a}\Omega r - \omega r_c\right)^2 rdr$$

Hence, the axial force in equation (42) can be rewritten as

$$\frac{1}{2}\rho W^2 B(2r_c)(C_L\cos\phi + C_D\sin\phi)dr = 4\pi\rho\left[U_\infty^2 a(1-a) + \frac{1}{4}\left(2\acute{a}\Omega r - \omega r_c\right)^2\right]rdr \tag{43}$$

or by some manipulations

$$\frac{W^2}{U_\infty^2}B\left(\frac{2r_c}{R}\right)(C_L\cos\phi + C_D\sin\phi) = \frac{8\pi r}{R}\left[a(1-a) + \frac{1}{4U_\infty^2}\left(2\acute{a}\Omega r - \omega r_c\right)^2\right] \tag{44}$$

The elemental tangential force in equation (34) is responsible for the generation of the torque over the blade element that expressed in equation (21). Thus, the elemental torque can be determined by

$$\begin{aligned}\delta Q &= rdF_T = \tfrac{1}{2}\rho W^2 B(2r_c)(C_L\sin\phi - C_D\cos\phi)rdr \\ &= 2\pi\rho U_\infty(1-a)\left(2\Omega\acute{a}r - \omega r_c\right)r^2dr\end{aligned} \tag{45}$$

which is simplified to

$$\frac{W^2}{U_\infty^2}B\left(\frac{2r_c}{R}\right)(C_L\sin\phi - C_D\cos\phi) = \frac{4\pi r}{RU_\infty}(1-a)\left(2\Omega\acute{a}r - \omega r_c\right) \tag{46}$$

Dividing equation (44) by equation (46), one can obtain

$$\frac{C_L\cos\phi + C_D\sin\phi}{C_L\sin\phi - C_D\cos\phi} = \frac{\frac{8\pi r}{R}\left[a(1-a) + \frac{1}{4U_\infty^2}\left(2\acute{a}\Omega r - \omega r_c\right)^2\right]}{\frac{4\pi r}{RU_\infty}(1-a)\left(2\Omega\acute{a}r - \omega r_c\right)} \tag{47}$$

Using dimensionless quantities explained so far and by defining the drag to lift ratio $\varepsilon = C_D/C_L$, one may obtain after some simplification

$$\frac{1+\varepsilon\tan\phi}{\tan\phi - \varepsilon} = \frac{2a(1-a) + \frac{1}{2}\left(2\acute{a}\lambda_r - \acute{\omega}\right)^2}{(1-a)\left(2\acute{a}\lambda_r - \acute{\omega}\right)} = \frac{2a}{\left(2\acute{a}\lambda_r - \acute{\omega}\right)} + \frac{\left(2\acute{a}\lambda_r - \acute{\omega}\right)}{2(1-a)} = Y \tag{48}$$

Inserting the optimum design values of $a = 1/3$ and $\acute{\omega}$ from equation (26), the Y function above is simplified to

$$Y(\lambda_r) = \frac{1}{(1-a)}\lambda_r + \frac{a}{\lambda_r} \tag{49}$$

which is simply a function of the axial induction factor, a, and the blade speed ratio, λ_r.

The drag to lift ratio ε can be obtained from experimental measurements. Hence, the relative wind angle over the rotor of the rotating cylinders is modified using the equation (48) as follow

$$\tan\phi = \frac{1+Y\varepsilon}{Y-\varepsilon} \tag{50}$$

Inserting at the limit of invisid solution, i.e. $\varepsilon = 0$, the variation of the relative wind angle φ obtained from equation (50) is identical to equation (33), which is

$$\phi = \tan^{-1}\left(\frac{1}{Y}\right) = \tan^{-1}\left(\frac{1-a}{\lambda_r + \frac{a(1-a)}{\lambda_r}}\right) \tag{51}$$

However, for non-zero values of the drag to lift ratio, ε, some modification on the angular induction factor must be implemented to satisfy both equations (50) and (32), simultaneously, as follow

$$\tan\phi = \frac{1+Y\varepsilon}{Y-\varepsilon} = \frac{1-a}{\left(1+\acute{a}\right)\lambda_r - \acute{\omega}/2} \tag{52}$$

By substituting $Y = (2a/(2\acute{a}\lambda_r - \acute{\omega})) + ((2\acute{a}\lambda_r - \acute{\omega})/2(1-a))$ from (48) in the above and rearranging equation (52) based on the angular induction factor, $\acute{a}$, one may arrive at the following cubic equation by some mathematical operations as

$$\begin{aligned}&pZ^3 + qZ^2 + sZ + t = 0\\ &p = \varepsilon\\ &q = -2\varepsilon\lambda_r\\ &s = \varepsilon(1-a)^2 + \lambda_r(1-a) + \varepsilon a(1-a) + \varepsilon\lambda_r^2\\ &t = -(1-a)^2(a + \varepsilon\lambda_r) - (1-a)\lambda_r^2\\ &Z = \left(1+\acute{a}\right)\lambda_r - \acute{\omega}/2\end{aligned} \tag{53}$$

Interestingly, it can be seen from equation (53) that the agular induction factor $\acute{a}$ may have three solutions based on the three roots of the cubic function for Z values, i.e. Z_1,Z_2, and Z_3, as follow

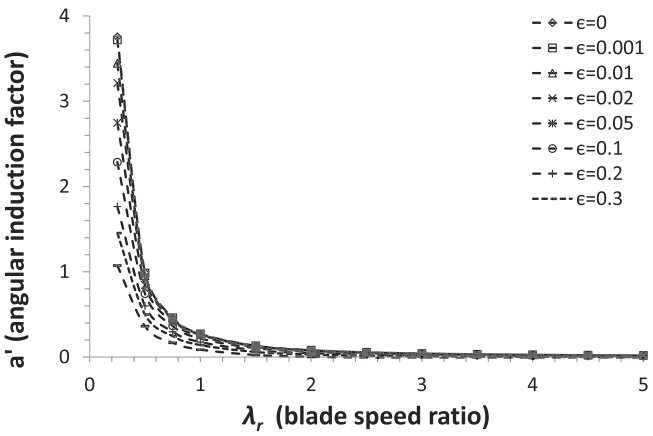

Fig. 14. The variation of the angular induction factor against the blade speed ratio at different values of the drag to lift ratio from the BEM theory.

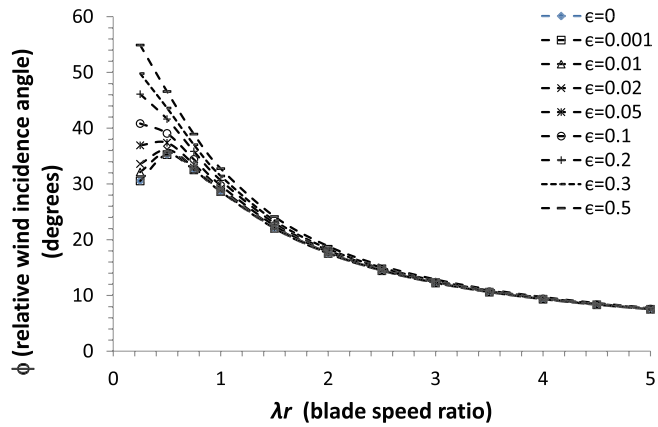

Fig. 15. The variation of the wind incidence angle against the blade speed ratio at different values of the drag to lift ratio from the BEM theory.

$$a' = -1 + \frac{Z + \acute{\omega}/2}{\lambda_r} \tag{54}$$

And more interestingly, the relative wind incidence angle φ is determined to be independent from spin ratio $\acute{\omega}$ as follows

$$\phi = \tan^{-1}\left(\frac{1-a}{Z}\right) \tag{55}$$

where Z is the root of the cubic function in (53) in which all its coefficients are independent of the spin ratio. The corrected angular induction factor should be determined from the roots of this cubic equation (53) to include the effects of viscosity based on the BEM theory. Equation (53) may contain complex roots which are nonphysical and should be discarded.

In Fig. 14, the effects of different values of the drag to lift ratio, ε, on the angular induction factor is shown for the constant spin ratio of, $\acute{\omega} = 0.1$. As seen in this figure, the angular induction factor is a decreasing function of the blade speed ratio λ_r. It is also observed that by increasing the drag to lift ratios, ε, from the value of zero to 0.5, the angular induction factor continuously decreases compared with the zero value ofε. The angular induction factor for higher drag to lift ratio may possess some negative values that may not have a physical meanings and further experimental validation or analytical studies is needed to give some insight into the physics of such conditions.

Based on the calculated angular induction factors shown in Fig. 14, it is expected that the results of the relative wind angle, shown in Fig. 12 at the case of inviscid flow $\varepsilon = 0$, to be changed for this viscous case of the BEM theory.

The results in Fig. 15 for the relative wind angle clearly shows the same trend of decreasing function with respect to the blade speed ratio λ_r. By increasing the drag to lift ratio, it is observed that the relative wind incidence angle is marginally enhanced in the vicinity of low values of the blade speed ratio, λ_r, up to the value of 3.

Next, for the higher value of the dimensionless spin ratio, the solutions to the cubic equation (53) are calculated to be identical for the relative wind incidence angle as discussed and proved by equation (55). While, the angular induction factors are calculated as monotonic increasing function of the spin ratio (see the equation (53)).

Hence, it is clearly evident that the spin ratio is not directly controlling the Magnus wind turbine performance since the wind relative incidence angle is independent from the spin ratio. However, the lift and drag of the Magnus blades are functions of the spin ratio as shown in Figs. 14 and 15. Thus, the BEM analysis takes into account indirectly the effects of the spin ratio by altering the drag to lift ratio. Note that it is assumed that the drag to lift ratio is constant across the blade because the lift force as well as the drag force increase along the blade. This is realistic because the spin ratio of the cylinder is constant along the blade and only the Reynolds number may slightly change from tip to root of the blade due to the increase of the relative wind speed.

4. The optimum power coefficient of Magnus type wind turbines

Another important feature of the wind turbine, i.e. power coefficient, is yet required to be determined from this analysis. One may define a local power coefficient, including the effects of drag force, for the annular element of rotor, $dA_d = 2\pi r dr$, as follows

$$C_{P_l} = \frac{\delta P}{\frac{1}{2}\rho U^3 dA_d} = \frac{\Omega \delta Q}{\frac{1}{2}\rho U_\infty^3 (2\pi r dr)} \tag{56}$$

The lift coefficient may be derived from the equation (44) as follows

$$r_c C_L = \left[a(1-a) + \left(\acute{a}\lambda_r - \frac{\acute{\omega}}{2}\right)^2\right] \frac{U_\infty^2}{W^2}\left(\frac{4\pi r}{B}\right) \frac{1}{\cos\phi(1+\varepsilon\tan\phi)} \tag{57}$$

The torque developed by the element of Magnus wind turbine over the elemental area dA_d may be taken from BEM analysis in equation (45) as follow

$$\delta Q = \frac{1}{2}\rho W^2 B(2r_c)(C_L\sin\phi - C_D\cos\phi) r dr \tag{58}$$

Inserting both equations (57) and (58) into the local power coefficient (56), one may obtain after some simplification

$$C_{P_l} = 4\lambda_r\left[a(1-a) + \left(\acute{a}\lambda_r - \frac{\acute{\omega}}{2}\right)^2\right]\left[\frac{\tan\phi - \varepsilon}{1+\varepsilon\tan\phi}\right] \tag{59}$$

Substituting $\acute{a}$ from equation (54), the above equation can be rewritten as

$$C_{P_l} = 4\lambda_r\left[a(1-a) + (Z-\lambda_r)^2\right]\left[\frac{\tan\phi - \varepsilon}{1+\varepsilon\tan\phi}\right] \tag{60}$$

Again, it is obvious from the above relation, the equation (53) on Z and also the equation (55) on the relative wind incidence angle φ

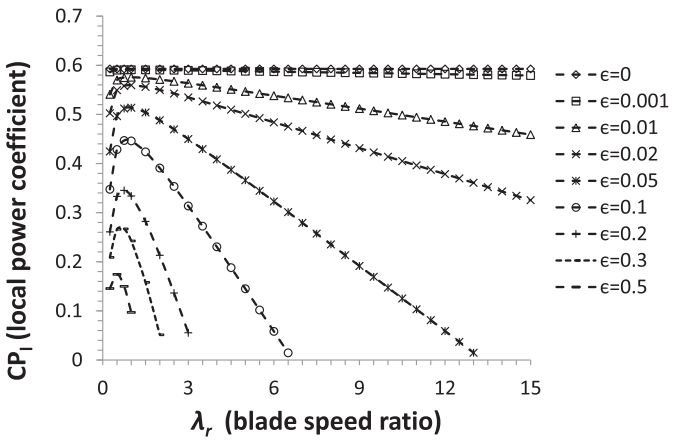

Fig. 16. The variation of the local power coefficient versus the blade speed ratio at different values of the drag to lift ratio from the BEM theory for any spin ratio.

that the local power coefficient is independent of the spin ratio or in fact it is not directly a dependent function of the spin ratioώ.

The total power gain from the wind turbine rotor may be integrated numerically from hub to tip radiuses as follows

$$C_{P_{tot}} = \frac{2}{\lambda^2}\int_{\lambda_h}^{\lambda} \lambda_r C_{P_l} d\lambda_r$$
$$= \frac{8}{\lambda^2}\int_{\lambda_h}^{\lambda} \lambda_r^2 \left[a(1-a) + \left(\acute{a}\lambda_r - \frac{\acute{\omega}}{2}\right)^2\right]\left[\frac{\tan\phi - \varepsilon}{1+\varepsilon\tan\phi}\right] d\lambda_r \quad (61)$$

where the blade tip speed ratio is denoted by $\lambda = R\Omega/U$. The effects of root and tip loss correction using the Prandtl correction factor, F, may also be implemented into the above analysis in equation (61).

Inserting the optimum design values of $a = 1/3$, and $\phi = \tan^{-1}(1 + Y\varepsilon/Y - \varepsilon)$, the results of the local power distribution given by equation (60) is shown in Fig. 16 for different values of drag to lift ratio and for any value of spin ratio ώ. It can be seen that the local power coefficient for the case of zero drag to lift ratio is independent from λ_r and is equals everywhere to the value of Betz limit; i.e. $C_{Pl} = 16/27$, which is valid theoretically.

As is the case for the aerofoil type commercial wind turbines, the parameter of drag to lift ratio is of fundamental importance to enhance power extraction from a wind turbine. It is likewise observed here from the Fig. 16 that the main challenge for the Magnus horizontal axis wind turbines is to reduce the drag to lift ratio.

5. Concluding remarks

The subject of using Magnus force from rotating bodies is fascinating many engineers and scientists to design innovative devices in aerospace and naval engineering. There is a renew interest in Flettner type ships in naval engineering due to increasing trends of fossil fuel costs and climate change concerns. There is also some success in development of Magnus type horizontal axis wind turbines in Japan which encouraged this research work. The subject of Magnus effects were extensively reviewed by Seifert who suggests that there are lack of specific methods and modelling available on how to design the lifting device from the Magnus effects. This paper is particularly concentrated on development and extension of models and theories that are usually used in wind energy community to design and to extend our understanding from the horizontal axis Magnus type wind turbines. It is well known that the drag to lift ratio is the most crucial parameter in designing and modelling the aerofoil type commercial type wind turbines; likewise, the findings of this research is also suggest that the success of any Magnus type horizontal axis wind turbine may be dependent on reducing the drag to lift ratio for large commercial application of Magnus effect in wind industry. The present power coefficient calculations for the Magnus wind turbine may show some merit for some small wind turbine applications; however, more experimental results on innovative application of Magnus effect is still needed to guarantee success of using Magnus force in large wind turbine applications. From the experimental results on drag and lift of spinning cylinders, the optimum value of drag to lift ratio is suggested equals to 0.2 which offers the power coefficient of 0.35 at the blade speed ratio of unity. This is not as yet promising for small wind turbine applications in low wind speeds unless designs such as Murakami's Magnus wind turbine with spiral ribs have someway tackled such poor performance.

References

[1] Seifert J. A review of the Magnus effect in aeronautics. Prog Aerosp Sci 2012;55:17–45.
[2] Bychkov NM, Dovgal AV, Kozlov VV. Magnus wind turbines as an alternative to the blade ones. J Phys Conf Ser 2007;75(012004):1–7.
[3] Murakami N, Akita JP, Ito J. Magnus type wind power generator, US Patent, 2007, 0046029:A1.
[4] Murakami N, Akita JP. Magnus type wind power generator, US Patent, 2010, 0038915:A1.
[5] Mecaro Co. Japan. <www.mecaro.jp/eng/> [accessed 11.01.13].
[6] Giudice F, La Rosa G. Design, prototyping and experimental testing of a chiral blade system for hydroelectric microgeneration. Mech Mach Theo 2009;44:1463–84.
[7] Reid EG. Tests of rotating cylinders. Flight 1925:17–20.
[8] Glauert MB. A boundary layer theorem, with applications to rotating cylinders. J Fluid Mech 1957;2(1):89–99.
[9] Ingham DB. Steady flow past a rotating cylinder. Comput Fluids 1983;II(4):351–66.
[10] Mittal S, Kumar B. Flow past a rotating cylinder. J Fluid Mech 2003;476:303–34.
[11] Tokumaru P, Dimotakis P. Rotary oscillation control of a cylinder wake. J Fluid Mech 1991;224:77–90.
[12] Badalamenti C, Prince SA. The effects of endplates on a rotating cylinder in crossflow. In: 26th AIAA Conf 2008. p. 7063.
[13] Thouault N, Breitsamter C, Seifert J, Badalamenti C, Prince SA, Adams NA. Numerical analysis of a rotating cylinder with spanwise discs. In: 27th International Congress of the aeronautical Sciences, ICAS 2010.
[14] Labraga L, Bourabaa N, Berkah T. Wall shear stress from a rotating cylinder in cross flow using the electrochemical technique. Exp Fluids 2002;33:488–96.
[15] Munson BR, Rothmayer AP, Okiishi TH, Huebsch WW. Fundamentals of fluid mechanics. 7th ed. Asia: John Wiley & Sons, Ltd; 2012.
[16] Burton T, Sharpe D, Jenkins N, Bossanyi E. Wind energy handbook. Chichester: John Wiley & Sons, Ltd; 2001.